

This article was downloaded by: [IRSTEA]

On: 29 September 2014, At: 06:57

Publisher: Taylor & Francis

Informa Ltd Registered in England and Wales Registered Number: 1072954

Registered office: Mortimer House, 37-41 Mortimer Street, London W1T 3JH, UK



## Aerosol Science and Technology

Publication details, including instructions for authors and subscription information:

<http://www.tandfonline.com/loi/uast20>

### Dispersion and Deposition of Spherical Particles from Point Sources in a Turbulent Channel Flow

Amy Li <sup>a</sup> & Goodarz Ahmadi <sup>a</sup>

<sup>a</sup> Department of Mechanical and Aeronautical Engineering, Clarkson University, Potsdam, NY, 13699  
Published online: 11 Jun 2007.

To cite this article: Amy Li & Goodarz Ahmadi (1992) Dispersion and Deposition of Spherical Particles from Point Sources in a Turbulent Channel Flow, *Aerosol Science and Technology*, 16:4, 209-226, DOI: [10.1080/02786829208959550](https://doi.org/10.1080/02786829208959550)

To link to this article: <http://dx.doi.org/10.1080/02786829208959550>

PLEASE SCROLL DOWN FOR ARTICLE

Taylor & Francis makes every effort to ensure the accuracy of all the information (the "Content") contained in the publications on our platform. However, Taylor & Francis, our agents, and our licensors make no representations or warranties whatsoever as to the accuracy, completeness, or suitability for any purpose of the Content. Any opinions and views expressed in this publication are the opinions and views of the authors, and are not the views of or endorsed by Taylor & Francis. The accuracy of the Content should not be relied upon and should be independently verified with primary sources of information. Taylor and Francis shall not be liable for any losses, actions, claims, proceedings, demands, costs, expenses, damages, and other liabilities whatsoever or howsoever caused arising directly or indirectly in connection with, in relation to or arising out of the use of the Content.

This article may be used for research, teaching, and private study purposes. Any substantial or systematic reproduction, redistribution, reselling, loan, sub-licensing, systematic supply, or distribution in any form to anyone is expressly

forbidden. Terms & Conditions of access and use can be found at <http://www.tandfonline.com/page/terms-and-conditions>

---

# Dispersion and Deposition of Spherical Particles from Point Sources in a Turbulent Channel Flow

Amy Li and Goodarz Ahmadi

*Department of Mechanical and Aeronautical Engineering,  
Clarkson University, Potsdam, NY 13699*

---

The dispersion and deposition of particles from a point source in a turbulent channel flow are studied. An empirical mean velocity profile and the experimental data for turbulent intensities are used in the analysis. The instantaneous turbulence fluctuation is simulated as a continuous Gaussian random field, and an ensemble of particle trajectories is generated and statistically

analyzed. A series of digital simulations for dispersion and deposition of aerosol particles of various sizes from point sources at different positions from the wall is performed. Effects of Brownian diffusion on particle dispersion are studied. The effects of variation in particle density and particle-surface interaction are also discussed.

---

## INTRODUCTION

Studies of aerosol particle motion and deposition on surfaces have attracted considerable attention in recent years due to their numerous industrial applications. An extensive review of particle diffusion in laminar flows was provided by Levich (1962). More recent studies in connection with microcontamination processes were presented by Cooper et al. (1986, 1989) and Liu and Kang-ho (1987). Cooper (1986) summarized the state of understanding of the microcontamination control in electronic industries. In turbulent flows, particles are transported by the mean motion and are dispersed by turbulence fluctuation and Brownian diffusion. Fuchs (1964), Davies (1966), Friedlander and Johnstone (1957), and Cleaver and Yates (1975) provided semi-empirical expressions for particle mass flux from a turbulent stream to smooth surfaces. Particle deposition to rough walls was studied by Browne (1974) and Wood (1981a). Extensive reviews on the subject were provided by Wood (1981b), Hidy (1984), and Papavergos and Hedley (1984).

The theory of Brownian diffusion was

formulated by Einstein (1903) and Uhlenbeck and Ornstein (1930). An extensive exposition of mathematical theory of Brownian motion was provided by Chandrasekhar (1943). Ahmadi (1972) studied the dispersion of Brownian charged particles in the presence of an applied uniform and nonuniform magnetic field.

Computational modeling of particle dispersion in turbulent flows was performed by Ahmadi and Goldschmidt (1970), Peskin (1975), Riley (1971), Maxey and Riley (1983), and McLaughlin (1989). Recently, Ounis and Ahmadi (1990) studied the dispersion of small particles in a numerically simulated random isotropic field. Rizk and Elghobashi (1985) analyzed motions of particles suspended in a turbulent flow near a plane wall. Abuzeid et al. (1989, 1991) used a simple simulation technique to study the deposition process of small, suspended particles in a turbulent channel flow.

In this article the process of deposition of dust particles released from a point source in a turbulent channel flow is studied. An empirical mean velocity profile and the experimental data for turbulent intensities are used.

Using a modified Gaussian random field model proposed by Kraichnan (1970), the instantaneous turbulent velocity field across the channel is numerically simulated. The Brownian motion is modeled as a white noise process. The particle equation of motion is solved and a number of particle trajectories are evaluated. Various trajectory statistics are computed and deposition of particles of various sizes is studied. The relative significance of turbulence and Brownian dispersion is also discussed. The effects of particle-surface interaction and particle density on particle deposition and dispersion are also studied.

### PARTICLE EQUATION OF MOTION

The equation of motion of a small aerosol particle including the lift force is given by

$$\begin{aligned} \frac{du_i^p}{dt} = & \frac{36\nu}{d^2(2S+1)C_c}(u_i - u_i^p) \\ & + \frac{2K\nu^{\frac{1}{2}}d_{ij}}{Sd(d_{lk}d_{kl})^{\frac{1}{2}}}(u_j - u_j^p) \\ & + \left(1 - \frac{1}{S}\right)g_i + n_i(t) \end{aligned} \quad (1)$$

and

$$\frac{dx_i}{dt} = u_i^p, \quad (2)$$

where,  $u_i^p$  is the velocity of the particle,  $x_i$  is its position,  $t$  is the time,  $d$  is the particle diameter,  $S$  is the ratio of particle density to fluid density,  $g_i$  is the acceleration of body force,  $n_i(t)$  is a Brownian force per unit mass,  $\nu$  is kinematic viscosity,  $K = 2.594$  is the constant coefficient of Saffman's lift force, and  $u_i$  is the instantaneous fluid velocity with  $u_i = \bar{u}_i + u_i'$ , where  $\bar{u}_i$  is the mean velocity of the fluid, and  $u_i'$  is its fluctuating component. In Eq. 1,  $C_c$  is the

Stokes-Cunningham slip correction given as

$$C_c = 1 + \frac{2\lambda}{d}(1.257 + 0.4e^{-1.1d/2\lambda}), \quad (3)$$

where  $\lambda$  is the molecular mean free path of the gas, and the deformation rate tensor  $d_{ij}$  is defined as

$$d_{ij} = \frac{1}{2}(u_{i,j} + u_{j,i}). \quad (4)$$

The lift force used in Eq. 1 is a generalization of the expression provided by Saffman (1965) for three-dimensional shear fields.

As was shown in Ounis and Ahmadi (1990), other hydrodynamical forces such as the Basset history, the virtual mass, the Faxen correction, and the pressure gradient are much smaller than the Stokes drag force for small particles. For aerosols in the range of 0.01 to 20  $\mu\text{m}$ , these forces are truly infinitesimal. Therefore, they were neglected in Eq. 1. The expression for the Saffman lift force that is included in Eq. 1 is restricted to small particle Reynolds number. In addition, the particle Reynolds number based on the particle-fluid velocity difference must be also smaller than the square root of the particle Reynolds number based on the shear field.

### SIMULATION OF TURBULENT FLOW FIELD

The mean velocity field in a turbulent channel flow as obtained in Ahmadi et al. (1976) is given by

$$\frac{\bar{u}}{\bar{u}_o} = \frac{1 - \eta^2 - \frac{k'_v}{k'} \frac{\cosh(k'\eta)}{\sinh k'} + \frac{k'_v \cosh k'}{k' \sinh k'}}{1 + \frac{k'_v \cosh k' - 1}{k' \sinh k'}}, \quad (5)$$

where  $\eta$  is the nondimensional distance from the center line,  $k'_v$  and  $k'$  are nondimensional parameters which are defined as

$$k'_v = \frac{0.00703 \text{Re}^{0.763}}{1 - 0.71 \text{Re}^{0.0134}} - 2, \quad (6)$$

$$k' = k'_v \frac{1 - 0.71 \text{Re}^{0.0134}}{0.71 \text{Re}^{0.0134}} - 0.5. \tag{7}$$

Here,  $\bar{u}_o$  is the mean centerline velocity and is given by

$$\bar{u}_o = V / (0.71 \text{Re}^{0.134}), \tag{8}$$

where  $V$  is the mean channel velocity and

$$\text{Re} = \frac{2\rho Vh}{\mu}, \tag{9}$$

is the Reynolds number. In Eq. 9  $h$  is the half width of channel,  $\rho$  is the fluid mass density, and  $\mu$  is the fluid viscosity. Good agreement between the predictions of Eq. 5 and the experiment data of Laufer (1953) was reported in Ahmadi et al. (1976). In this study, the mean velocity profile given by Eq. 5 is used.

Figure 1 shows distributions of the experimental data of Kreplin and Eckelmann

(1979) for turbulence intensities,  $e_1(y) = \sqrt{u'^2}/u^*$ ,  $e_2(y) = \sqrt{v'^2}/u^*$ ,  $e_3(y) = \sqrt{w'^2}/u^*$ , across the channel of a Reynolds number of 7700. In Figure 1 all intensities are nondimensionalized with respect to the shear velocity,  $u^* = \sqrt{\tau_o/\rho}$ , where  $\tau_o$  is the wall shear stress which is related to the friction factor  $f$ . That is,

$$f = \frac{4\tau_o}{\frac{1}{2}\rho V^2} = \frac{8u^{*2}}{V^2}. \tag{10}$$

Here, an empirical equation (White, 1986) for the friction factor  $f$  given by

$$\frac{1}{f^{1/2}} = -1.8 \log \left[ \frac{6.9}{2 \text{Re}} \right] \tag{11}$$

is used.

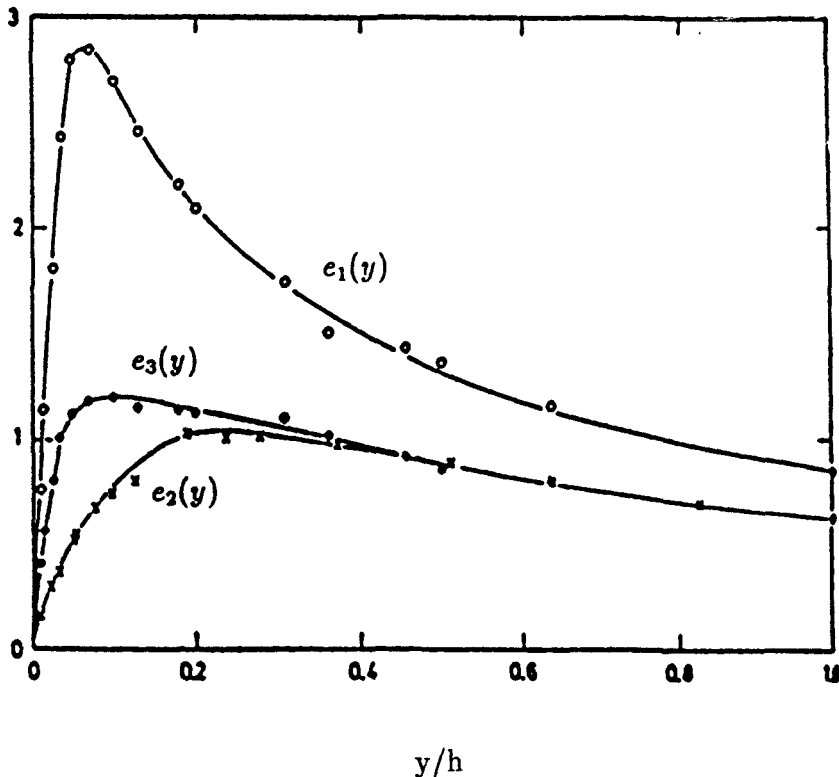


FIGURE 1. Distributions of nondimensional turbulence intensities.

The turbulence fluctuations are random functions of space and time. The Monte Carlo velocity simulation techniques have been used as an economical method for generating time histories that have the random characters and statistical properties of turbulence. Kraichnan (1970) suggested a simple method for generating a Gaussian random field which resembles a pseudo-isotropic turbulence. Accordingly, the instantaneous fluctuating velocity is given as

$$\begin{aligned} \vec{u}^{I*}(\vec{x}^*, t^*) &= \sqrt{\frac{2}{N}} \left\{ \sum_{n=1}^N \vec{u}_1(\vec{k}_n) \right. \\ &\quad \times \cos(\vec{k}_n \cdot \vec{x}^* + \omega_n t^*) \\ &\quad \left. + \sum_{n=1}^N \vec{u}_2(\vec{k}_n) \sin(\vec{k}_n \cdot \vec{x}^* + \omega_n t^*) \right\}. \end{aligned} \tag{12}$$

In this equation

$$\vec{u}_1(\vec{k}_n) = \vec{\xi}_n \times \vec{k}_n, \quad \vec{u}_2(\vec{k}_n) = \vec{\xi}_n \times \vec{k}_n, \tag{13}$$

with

$$\vec{k}_n \cdot \vec{u}_1(\vec{k}_n) = \vec{k}_n \cdot \vec{u}_2(\vec{k}_n) = 0, \tag{14}$$

ensure the incompressibility condition. The components of vectors  $\vec{\xi}_n$  and  $\vec{\xi}_n$  and the frequencies  $\omega_n$  are picked independently from a Gaussian distribution with a standard deviation of unity. Each component of  $\vec{k}_n$  is a Gaussian random number with a standard deviation of  $1/\sqrt{2}$ . Here,  $N$  is the number of terms in the series.

In Eq. 12 the dimensionless quantities are defined as

$$x^* = \frac{x}{l_o}, \quad t^* = \frac{t}{t_o}, \quad u_i^{I*} = \frac{u_i^{I'}}{u_i^*}, \tag{15}$$

where  $l_o$ ,  $t_o$ , and  $u_i^*$  are local scales of turbulence and  $u_i^{I'}$  is the fluctuation fluid velocity that is assumed to be isotropic. For this pseudoturbulent velocity field the en-

ergy spectrum  $E(k)$  is given by

$$E(k) = 16(2/\pi)^{1/2} k^4 e^{-2k^2} \tag{16}$$

The experimentally measured root-mean-square (RMS) fluctuation velocities shown in Figure 1 are clearly nonisotropic. In this study the fluctuation velocity given by Eq. 12 is modified to make it suitable for generating the nonisotropic instantaneous velocity field in the channel. It is assumed that

$$u_i' = u_i^{I'} e_i(y), \quad (\text{no sum on } i) \tag{17}$$

where  $e_i(y)$  are the shape functions for the axial, vertical, and transverse RMS velocities as given in Figure 1. (Here 1, 2, and 3 stand for the  $x$ ,  $y$ , and  $z$  directions, respectively.)

Normal component of turbulence fluctuations near a wall has a profound effect on the deposition rate of particles. Therefore, the magnitude of  $e_2(y)$  must be correctly evaluated for small values of  $y$ . It is well known (Hinze, 1975) that  $v'$  has a quadratic variation at short distances from the wall, i.e.,

$$v' \sim y^2 \text{ as } y^+ \rightarrow 0. \tag{18}$$

In this study

$$e_2(y) = Ay^{+2} \text{ as } y^+ \rightarrow 0, \tag{19}$$

with  $A = 0.0278$  is used to match the data given in Figure 1. Here

$$y^+ = yu^*/\nu, \tag{20}$$

is the distance from the wall in wall units, and  $\nu = \mu/\rho$  is the kinematic viscosity of fluid.

Estimates for the length and time scales of turbulence for wall-bounded flows were provided in Davies (1972). Accordingly,

$$l_o = 0.1 h (2 \text{Re})^{-1/8}, \tag{21}$$

and

$$t_o = \frac{l_o}{u^*} = \frac{2h}{20u^*(2\text{Re})^{1/8}} = \frac{h}{2V}. \tag{22}$$

Equations 12 and 17 with  $N = 100$  together with Eqs. 21 and 22 are used for simulating the fluctuation components of turbulent velocity in the channel. Sample space

and time variations of fluctuation velocity components are shown in Figure 2. The random characters of the fluctuation velocity fields are clearly observed from Figure 2. Here,

$$t^+ = \frac{tu^{*2}}{\nu} \quad (23)$$

is the dimensionless time and  $\nu/u^{*2}$  is the wall unit for time. For present simulations a time wall unit of  $\nu/u^{*2} = 1.67 \times 10^{-4}$  s is used. Figure 2b also shows that the axial velocity fluctuation is much larger than that in the vertical direction near the wall. At the centerline, however, the fluctuation velocities have roughly the same intensity.

**BROWNIAN MOTION**

For submicron particles the effect of Brownian motion becomes significant. To include such effects in the simulation the Brownian force  $n_i(t)$  is modeled as a Gaussian white noise random process (Uhlenbeck and Ornstein, 1930; Chandrasekhar, 1943; Ounis et al., 1991; Gupta and Peters, 1985) with spectral intensity  $S_{ij}^n$  given by

$$S_{ij}^n = S_o \delta_{ij}, \quad (24)$$

where

$$S_o = \frac{216\nu kT}{\pi^2 \rho d^5 S^2 C_c} \quad (25)$$

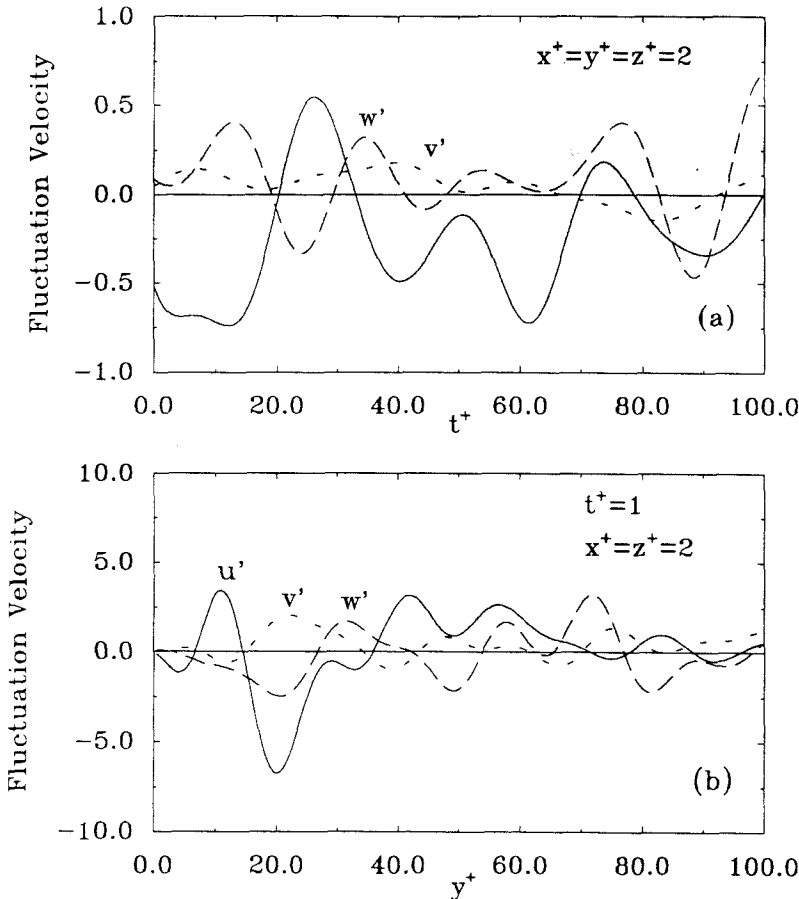


**FIGURE 2.** Sample time and space variations of fluctuation velocity components.

Downloaded by [IRSTEA] at 06:57 29 September 2014

Here,  $T$  is the absolute temperature of fluid, and  $k = 1.38 \times 10^{-23} \text{ J/K}$  is the Boltzmann constant. Amplitudes of the Brownian force components at every time step are then evaluated from

$$n_i(t) = G_i \sqrt{\frac{\pi S_o}{\Delta t}}, \quad (26)$$

where  $G_i$  is zero-mean, unit variance independent Gaussian random numbers and  $\Delta t$  is the time step used in the simulation.

To verify the adequacy of simulation procedure for Brownian motion, the example of diffusion of massless particles from a point source is studied. For a constant mean velocity  $V$ , Goldman and Marchello (1969), among others, analyzed this problem and obtained a close form solution for the RMS

lateral particle displacement. Accordingly, 
$$\sigma_y = \sqrt{2Dx/V}, \quad (27)$$

where  $D$  is the Brownian diffusivity given by

$$D = \frac{kT}{2\pi\mu d} C_c. \quad (28)$$

Five-hundred massless particle trajectories were generated, and ensemble averaging were used and RMS particle displacements were evaluated. The variation of the exact RMS displacement as given by Eq. 27 is shown in Figure 3. It is observed that the simulation results are in good agreement with the prediction of Eq. 27.

An alternative procedure for simulation of Brownian motion was described by Gupta

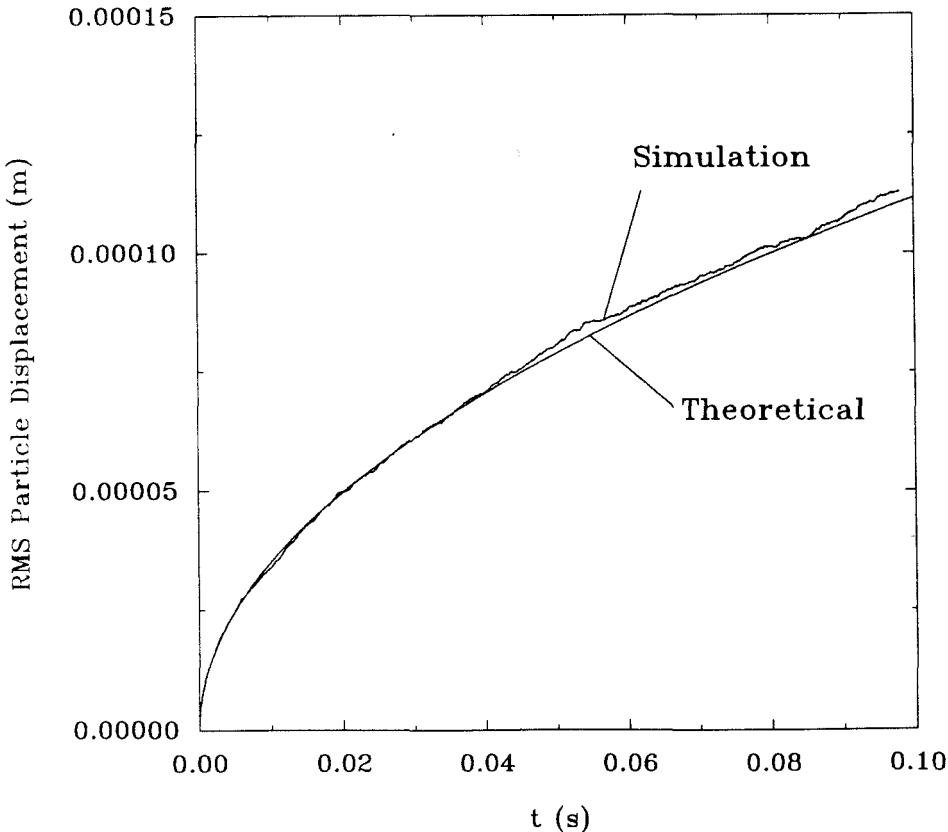


FIGURE 3. Root-mean-square particle displacement versus time.

and Peters (1985). Their method is based on the solution of the corresponding Fokker-Planck equation for a small time step. In the present method, however, the Brownian force is directly simulated as a white noise process and is added to the equation of motion of the particle. As a result, it is somewhat simpler than the technique of Gupta and Peters (1985) and it is more flexible in that the coupling effects with other forces could be easily accounted for.

### PARTICLE-SURFACE INTERACTIONS

At low impact velocities, particles that strike a surface will adhere to it. But as the impact velocity increases, the particle may rebound from the surface. Bounce occurs when the kinetic energy of a particle is sufficiently large to escape the attractive forces at the surface. The collision of a particle and a surface can be conveniently characterized in terms of the energy of particle-surface interaction (Friedlander, 1977; Dahneke, 1971, 1972; Davis et al., 1986). Let  $V_{1\infty}$  be the particle normal approach velocity, and  $E$  be the surface potential energy. The energy of the particle near the surface before and after impact are given, respectively, by  $mV_{1\infty}^2/2 + E_1$  and  $mV_{2\infty}^2/2 + E_2$ . Here,  $V_{2\infty}$  and  $E_2$  are the normal velocity and potential energy after collision, respectively. Neglecting energy dissipation through viscous damping (for a collision in vacuum in the absence of lubrication film), we have (Friedlander, 1977)

$$\frac{V_{1\infty}}{V_{2\infty}} = \left[ r^2 - \frac{E_2 - r^2 E_1}{mV_{1\infty}^2/2} \right]^{\frac{1}{2}}, \quad (29)$$

where  $r$  is the coefficient of restitution.

When  $V_{2\infty} = 0$ , a particle cannot escape the surface force field. For  $E_1 = E_2 = E$ , the critical approach velocity corresponding to  $V_{2\infty} = 0$  is given by

$$V_{1c} = \left[ \frac{2E}{m} \left( \frac{1 - r^2}{r^2} \right) \right]^{\frac{1}{2}}. \quad (30)$$

Thus, capture or bouncing will occur when  $V_{1\infty}$  is less or greater than  $V_{1c}$ .

According to Dahneke (1971, 1972), the surface potential energy is given by

$$E = \frac{Ad}{12y_0}, \quad (31)$$

where  $A$  is the Hamaker constant,  $y_0$  is the equilibrium separation of a particle and a surface (typically  $y_0 = 4 \text{ \AA}$ ), and  $d$  is the diameter of the particle. The Hamaker constants for several materials were given by Dahneke (1972).

### RESULTS AND DISCUSSION

Simulation results for dispersion and deposition of aerosol particles from a point source in a 2-cm wide channel are described in this section. A mean air velocity of  $V = 5.0 \text{ m/s}$  in the channel is considered. A temperature of  $288 \text{ K}$ ,  $\mu = 1.84 \times 10^{-5} \text{ N}\cdot\text{s/m}^2$  and  $\rho = 1.225 \text{ kg/m}^3$  for air are used. The flow Reynolds number based on the channel width is 6657. Thus, the air is in a state of turbulent motion. The friction velocity under these flow conditions is  $0.3 \text{ m/s}$ . At this Reynolds number the thickness of one wall unit ( $\nu/u^*$ ) is about  $50 \text{ }\mu\text{m}$  and the half width of the channel in wall units is about 200. For a density ratio of  $S = 2000$ , different particle diameters and various point source distances from the wall are used and particle dispersion is analyzed. Particle trajectories were evaluated by solving Eqs. 1 and 2 using a finite difference method. For particles larger than a few micron, the time step  $dt$  must be smaller than the particle relaxation time. For submicron particles for which the inertia effect is negligible, such a limitation is impractical and unnecessary. The simulation results, however, showed that the trajectory statistics remain the same when the time step is less than certain values. A time step of  $0.0001 \text{ s}$  was found to give satisfactory results for the present simulations.

Ensembles of 1000 samples are employed for evaluating various particle trajectory

statistics and wall deposition rates. The results for trajectory statistics including the maximum and minimum trajectories are plotted in several figures. It should be emphasized that the absolute maximum and minimum trajectories depend on the ensemble size used. Nevertheless, they provide a visual display of the spreading rate. In addition, whenever the minimum curve touches the wall, it indicates that a particle reached the surface boundary.

Figure 4 shows the time variations of various forces for a  $5\text{-}\mu\text{m}$  particle. It is observed that the drag is the dominant force. The lift force is, generally, about 5% to 10% of the drag force. However, for certain time duration, the lift force may become

comparable to the drag force. The Brownian force is very small for  $5\text{-}\mu\text{m}$  particles.

Figure 5 displays variations of particle trajectory statistics for different diameters from a point source at a distance of 10 wall units (0.50 mm). the channel is horizontal and the gravitational force which is perpendicular to the flow direction is included in the simulation. The dispersion of various size particles is clearly observed from this figure. Figure 5a shows that the mean particle path for  $5\text{-}\mu\text{m}$  particles remains at about 10 wall units. Figure 5b and c shows that the mean trajectories for  $1\text{-}\mu\text{m}$  and  $0.01\text{-}\mu\text{m}$  particles moves away from the wall as time increases. This indicates that the gravitational effect is not significant for these latter

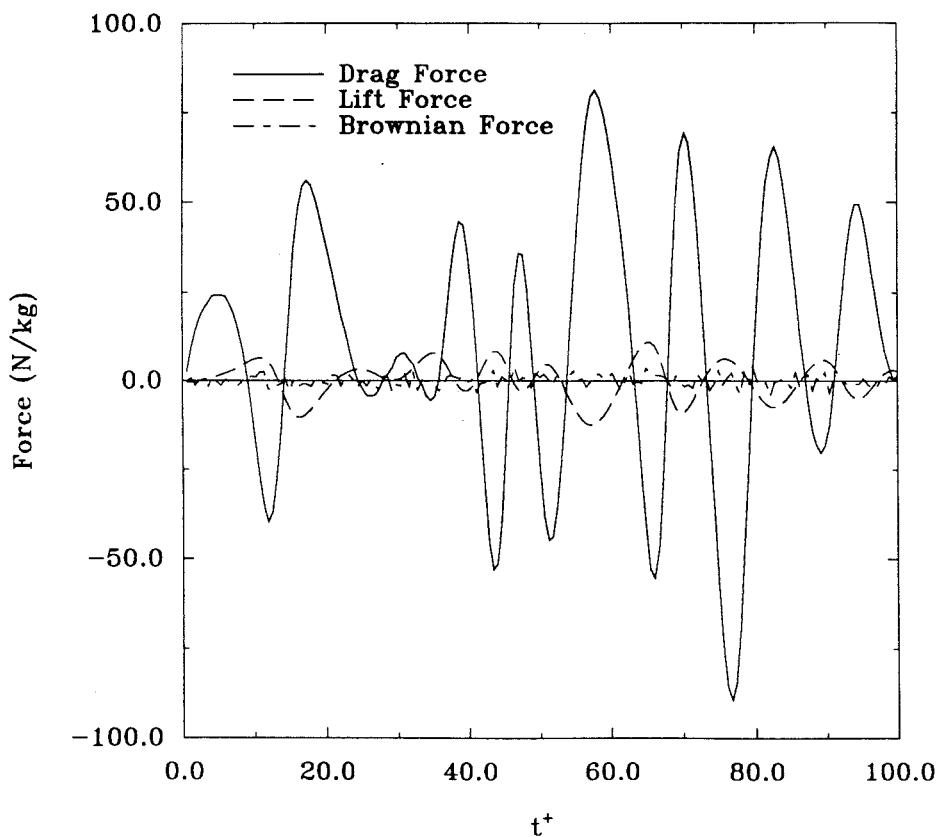


**FIGURE 4.** The time variations of various forces for a  $5\text{-}\mu\text{m}$  particle.

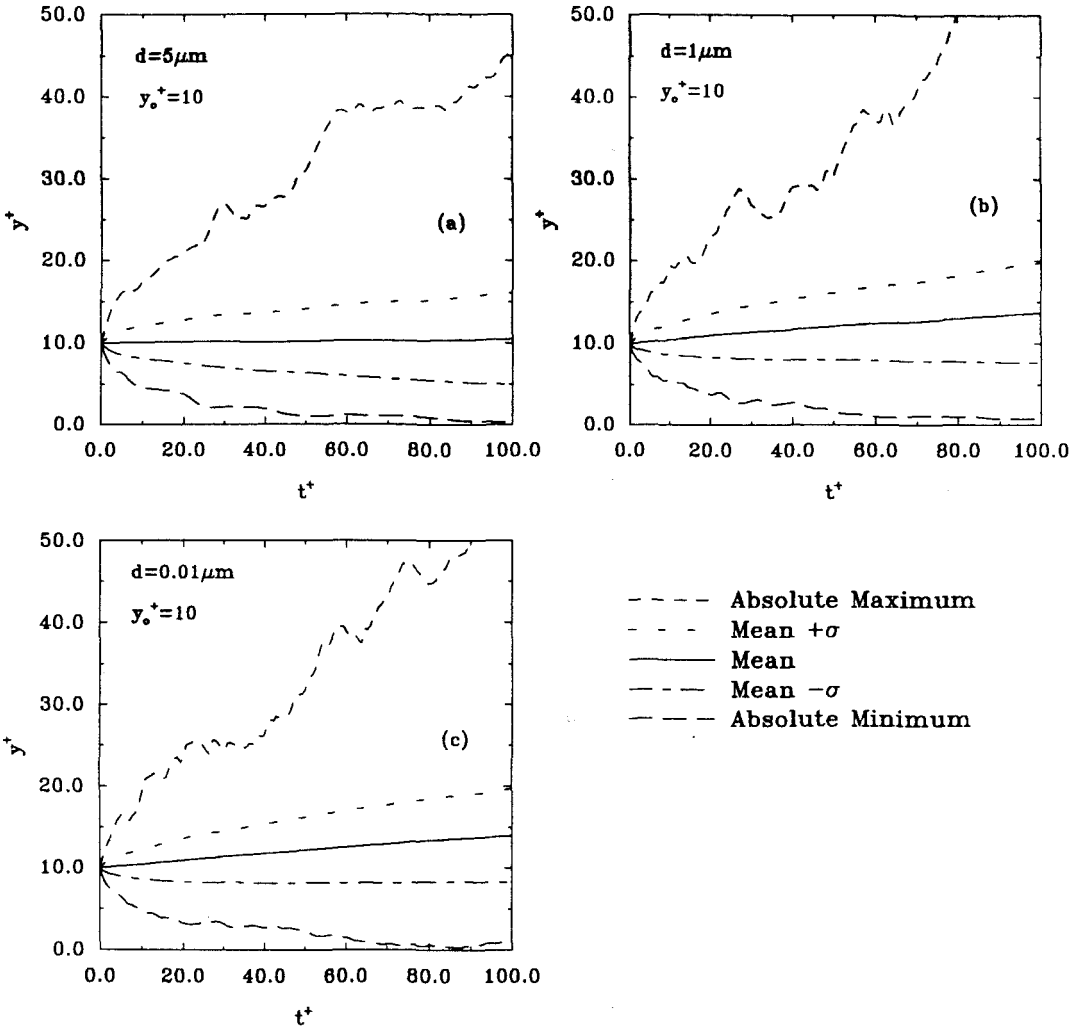


**FIGURE 5.** Particle trajectory statistics for  $y_o^+ = 10$ . (a)  $d = 5 \mu\text{m}$ ; (b)  $d = 1 \mu\text{m}$ ; (c)  $d = 0.01 \mu\text{m}$ .

particles. From Figure 5 it is observed that all these different particles have quite similar trajectory statistics and spread by roughly  $\pm 6$  wall units at  $t^+ = 100$ . This observation shows that, when aerosol particles are not too close to a wall, turbulence is the dominating dispersion mechanism and the effects of Brownian motion and gravity are negligible.

Figure 6 shows the trajectory statistics of different particles that are released from a

point source at a distance of 1 wall unit from the wall. The particle spreading rates differ significantly from one another in this case. Figure 6a shows that the mean trajectory for 5- $\mu\text{m}$  particles is almost straight. The standard deviation at  $t^+ = 100$  is only about 1 wall unit.

Figure 6b and c shows that the mean distances from the wall gradually increase with time for 1- $\mu\text{m}$  and 0.01- $\mu\text{m}$  particles. The spreading rate for 1- $\mu\text{m}$  particles is

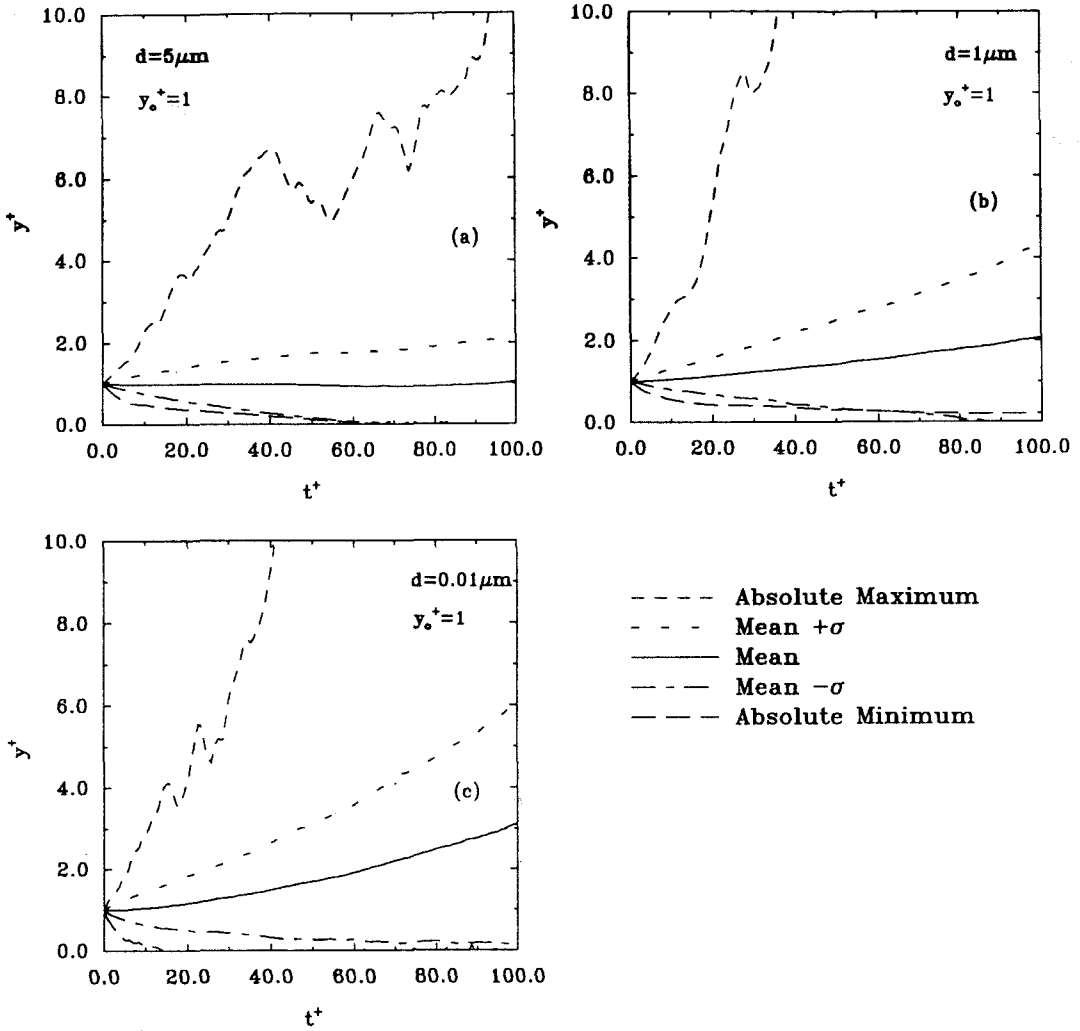


FIGURE 6. Particle trajectory statistics for  $y_o^+ = 1$ . (a)  $d = 5 \mu\text{m}$ ; (b)  $d = 1 \mu\text{m}$ ; (c)  $d = 0.01 \mu\text{m}$ .

about  $\sigma = 2$  at  $t^+ = 100$ . However, their diffusion toward the wall is quite slow and no particle is deposited on the wall in this time duration. The  $0.01\text{-}\mu\text{m}$  particles, however, are dispersed significantly, and Figure 6c shows that more than 265 particles are deposited on the wall in the time duration of 100 wall units. The reason for these widely different dispersion behaviors may be explained as follows. Very near the wall, the turbulent fluctuation dies down and the

Brownian motion becomes the dominant mechanism for diffusion of particles less than  $0.1 \mu\text{m}$ . Brownian dispersion effect for particles larger than  $0.5 \mu\text{m}$  is negligibly small. Thus, large particles that are trapped near the wall cannot diffuse to the wall. The larger ones ( $d \approx 5 \mu\text{m}$ ) will deposit rapidly on the wall due to gravitational sedimentation. Aerosols of the order of  $0.5$  to  $1 \mu\text{m}$  will remain suspended for a relatively long time without being deposited on the surface

due to the absence of significant dispersing mechanisms.

The particle trajectory statistics in a turbulent channel flow in the absence of gravity are also studied. The particles are released at a distance 1 wall unit from the wall, and the results are shown in Figure 7. This figure shows that 5- $\mu\text{m}$  and 1- $\mu\text{m}$  particles spread about  $\pm 1.5$  and 2 wall units with respect to their mean in the time duration of 100 wall units. The 0.01- $\mu\text{m}$  particles, how-

ever, spread about 3 wall units due to their significant Brownian motions. Comparing Figures 6 and 7, it is observed that the trajectory statistics for 0.01- $\mu\text{m}$  and 1- $\mu\text{m}$  particles are not affected by the presence of gravity. For 5- $\mu\text{m}$  particles, however, the gravitational sedimentation effects significantly alter the trajectory statistics. Figure 7a shows that none of the 5- $\mu\text{m}$  particles are deposited when the gravitation field is absent.

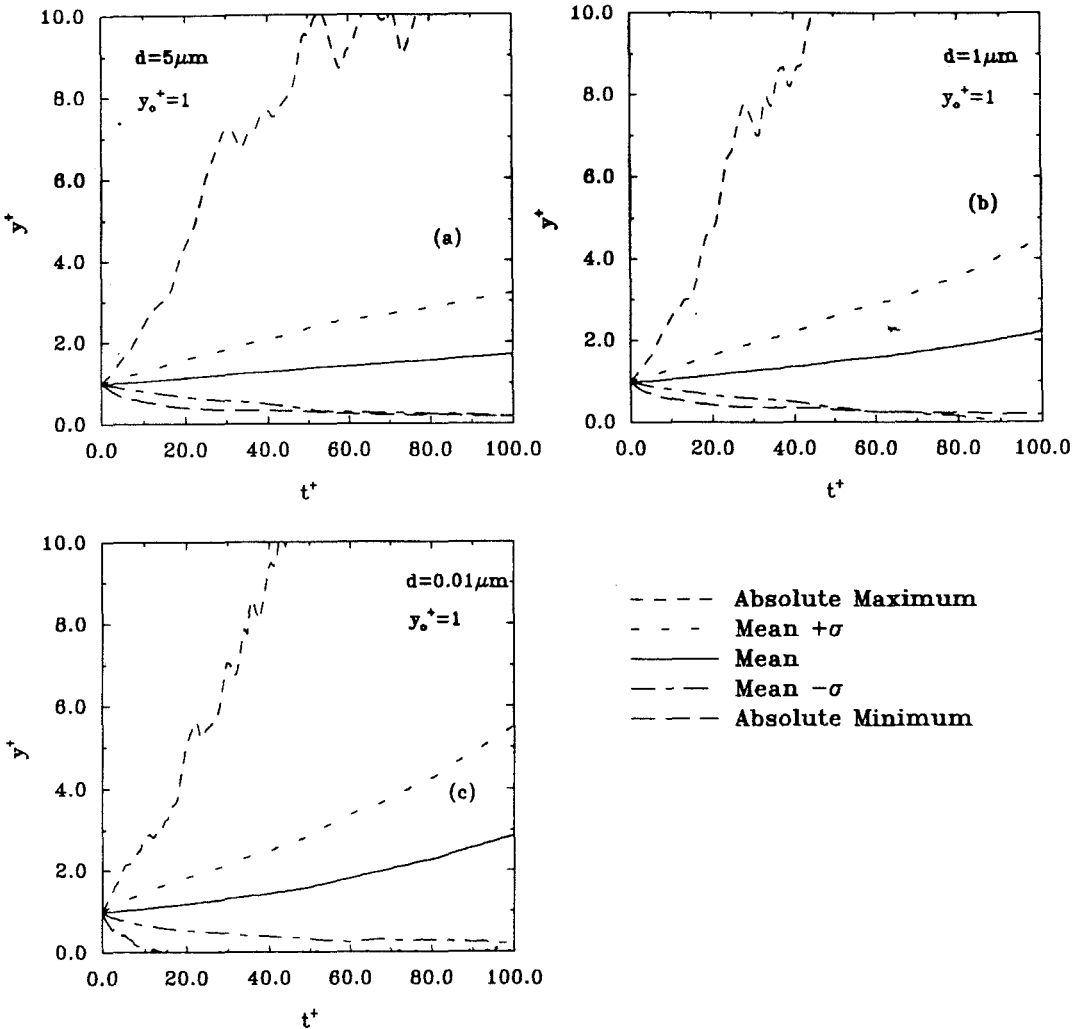


**FIGURE 7.** Particle trajectory statistics in absence of gravity for  $y_0^+ = 1$ . (a)  $d = 5 \mu\text{m}$ ; (b)  $d = 1 \mu\text{m}$ ; (c)  $d = 0.01 \mu\text{m}$ .

Figure 8 displays sample trajectories for gravitational sedimentation of 5- $\mu\text{m}$  and 3- $\mu\text{m}$  particles. To understand the effects of different dispersion mechanisms, simulations for the cases in which turbulence or Brownian or when both effects are absent are performed. It is observed that in the absence of turbulence or Brownian effects, 5- $\mu\text{m}$  and 3- $\mu\text{m}$  particles follow straight paths and reach the wall at  $t^+$  of about 140 and 900 wall units, respectively. Figure 8a shows, for 5- $\mu\text{m}$  particles, the Brownian motion is negligible and the effect of turbulence is small. These particles essentially follow the

gravitational sedimentation trajectory within the 1 wall unit from the wall. Figure 8b shows that the Brownian effect on 3- $\mu\text{m}$  particles is quite small. The turbulence, however, significantly alters the particle path for a 3- $\mu\text{m}$  particle. From the trajectories shown in Figure 8b, it appears that the turbulence fluctuation effects remain noticeable up to about 0.4 wall units from the wall.

Figure 9 shows the number of particles that deposit on the wall versus time. Ensembles of 1000 particle trajectories for a point source at 1 wall unit from the wall and a

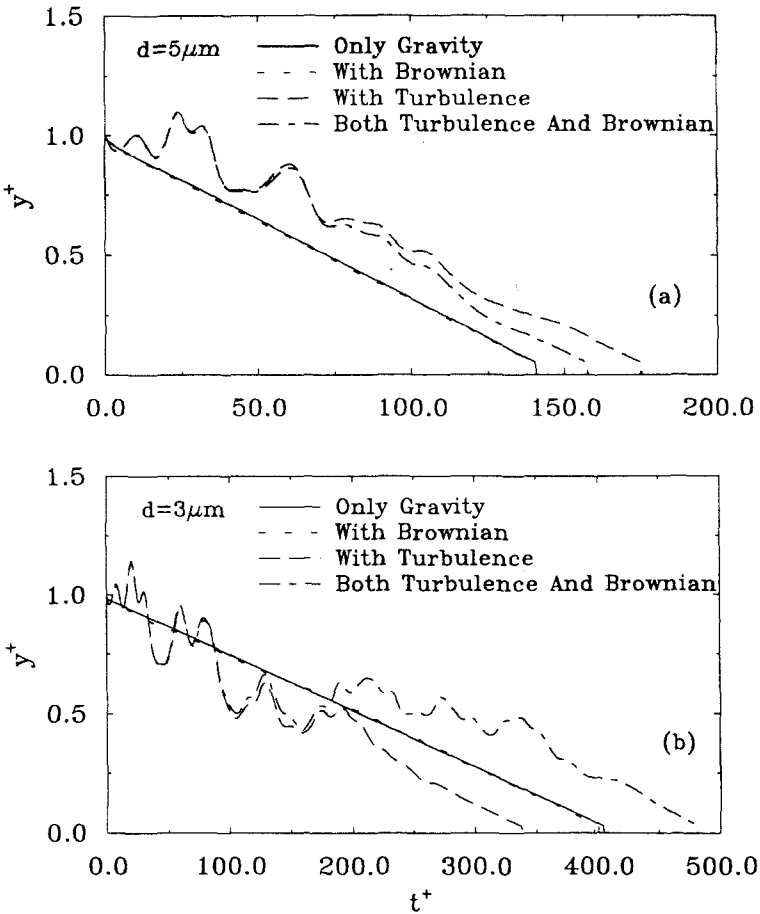


**FIGURE 8.** Sample trajectories for gravitational sedimentation and effects of turbulence and Brownian motion. (a)  $d = 5 \mu\text{m}$ ; (b)  $d = 3 \mu\text{m}$ .

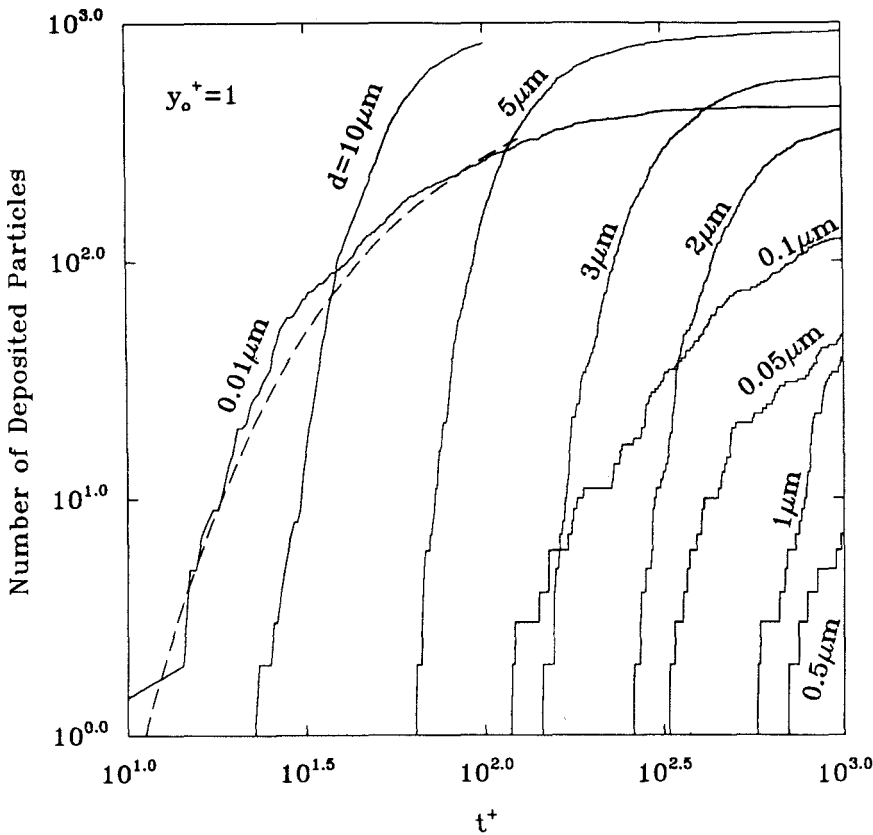


**FIGURE 9.** Number of deposited particles versus time for  $S = 2000$  and an ensemble of 1000 trajectories.

time duration of 1000 wall units (about 0.17 s) were used in these simulations. The numbers next to different curves identify the corresponding particle diameter. It is observed that the variation of the number of deposited particles for  $d \geq 0.5$  have rather sharp gradients. For example, about 800 5- $\mu\text{m}$  particles deposit on the wall in the time interval of 80 to 300 wall units. About 450 3- $\mu\text{m}$  particles deposit in the time intervals of  $200 < t^+ < 500$ . The sedimentation velocities for 5- $\mu\text{m}$  and 3- $\mu\text{m}$  particles are about 0.182 cm/s (0.0072 wall units) and 0.065 cm/s (0.0026 wall units), respectively. Thus, for  $t^+$  of about 140 and 390, these particles sediment by about one wall unit.

The results shown in Figure 9 indicate that for particles larger than 3  $\mu\text{m}$ , deposition occurs mainly around the time that particles are expected to reach the wall by the sedimentation velocity. For smaller particles the deposition rate decreases. The minimum deposition rate occurs for 0.5- $\mu\text{m}$  particles. As particle diameters decrease further beyond 0.5  $\mu\text{m}$ , the Brownian motion effect becomes significant. Figure 9 shows that about 50 0.1- $\mu\text{m}$  particles are deposited on the wall while more than 450 0.01- $\mu\text{m}$  particles reach the wall during the time interval shown in Figure 9. The dotted line in this figure is the total number of deposited particles released from a point source for 0.01- $\mu\text{m}$  particles given by the

simple Brownian theory of Ounis et al. (1991). A good agreement between the present simulation and theory is observed for 0.01- $\mu\text{m}$  particles.

It is perhaps of interest to discuss the effect of turbulence on particle deposition process. Turbulence will spread the particles and enhance the deposition rate. For laminar flows the graphs for time evolution of number of deposited particles with diameters larger than a few micron become unit step functions. In contrast, Figure 8 shows that turbulence causes a smooth-diffusionlike deposition rate. The effect of turbulence becomes particularly noticeable when the gravitational effect is absent. In this case

turbulence eddy-impaction becomes the main deposition mechanism. As a result, the deposition rate increases with particle size (for  $d > 2 \mu\text{m}$ ). For laminar flows the particle deposition decreases sharply with an increase in particle diameter.

Figure 10 shows the number of particles that are deposited in the time duration of 1000 wall units versus diameter. It is observed that the variation follows a V-shaped curve. That is, the deposition rates are rather high for both very large and very small particles. The minimum deposition rate occurs for particle diameter of 0.5  $\mu\text{m}$  for the flow condition used in this study. The V-shape behavior of the deposition is con-

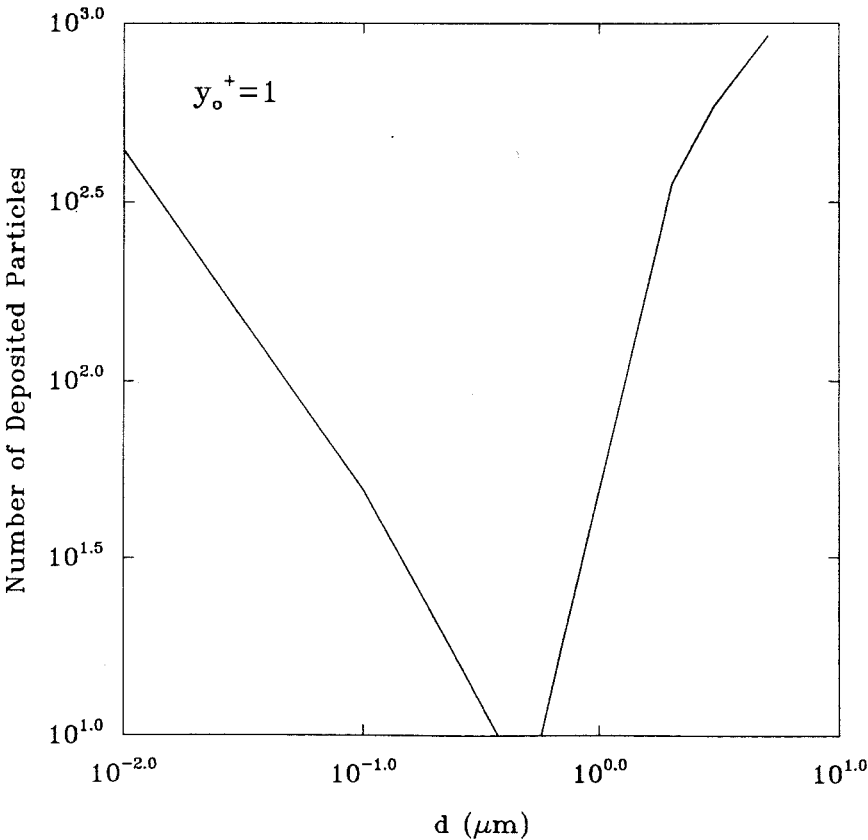
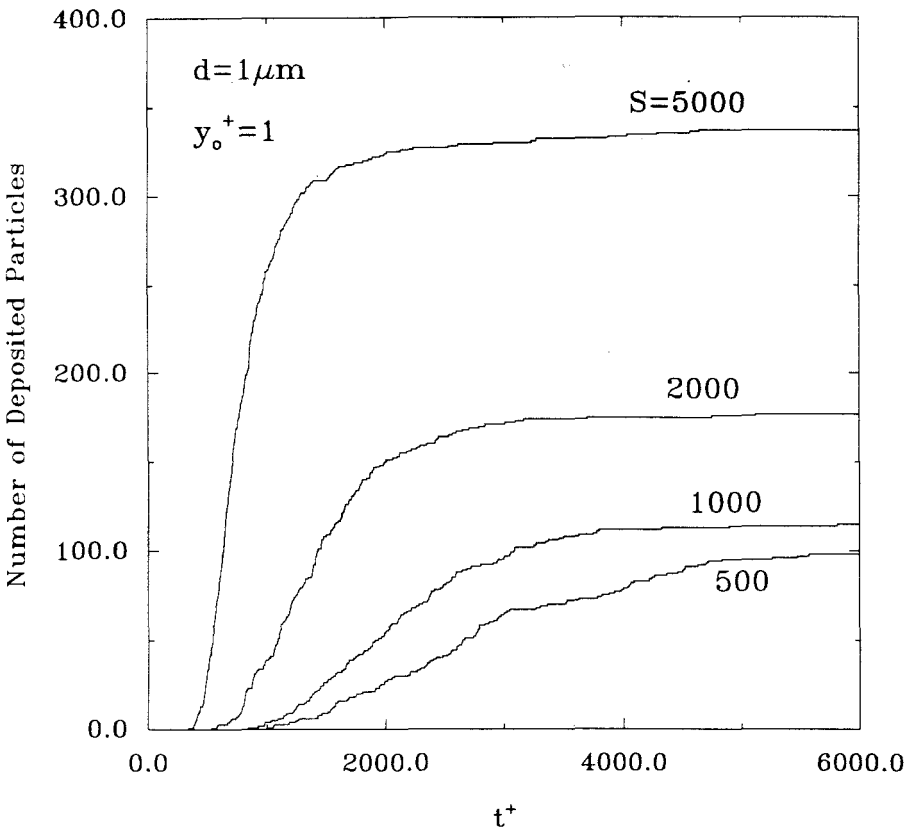


**FIGURE 10.** Number of deposited particles versus diameter for  $S = 2000$  and an ensemble of 1000 trajectories.

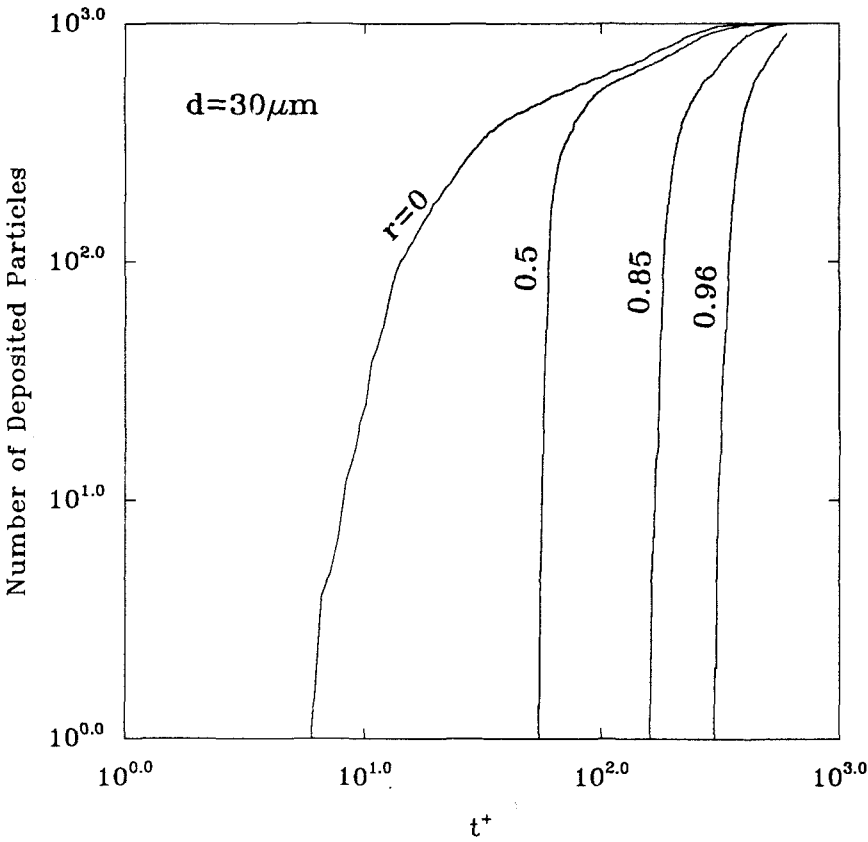
sistent with the trend of variation of experimental data of Sehmel (1973). For submicron particle the Brownian diffusion dominates the particle deposition process, whereas gravitational sedimentation and turbulence eddy-impaction are the controlling mechanisms for deposition of large particles.

Figure 11 shows the effect of density on the deposition rate of  $1\text{-}\mu\text{m}$  particles that are released from a point source at a distance of 1 wall unit from the wall. The simulation results show that the number of deposited particles increases rapidly with particle density. In the time duration of 6000 wall units, more than 330 particles with  $S = 5000$  are deposited on the wall, while only 98 particles with a density ratio of 500 reach the wall.

Variations of numbers of deposited particles with nondimensional time for  $30\text{-}\mu\text{m}$  silicon particles from a point source at a distance of 10 wall units from the wall in a horizontal channel are displayed in Figure 12. The surface is assumed to be coated by a layer of gold, and a value of the Hamaker constant  $A = 31.60 \times 10^{-10} J$  for silicon-gold interface, as suggested by Dahneke (1972), is used. Several coefficients of restitution, including  $r = 0$  (no rebound), are also considered. It is observed that the particle rebound from the surface significantly reduces the number of deposited particles within a given initial time duration. Furthermore, the time that the first particle deposits on the wall also increases considerably. For coefficients of restitution of 0.5, 0.85, and 0.96, the time that the first  $30\text{-}\mu\text{m}$



**FIGURE 11.** Number of deposited particles versus time for  $y_0^+ = 1$  and an ensemble of 1000 trajectories.



**FIGURE 12.** Number of deposited particles versus time for  $d = 30 \mu\text{m}$  including the effect of particle-surface interaction.

silicon particle deposits on the wall is about 60, 170, and 300 wall units of time, respectively. In the case of no rebound effect ( $r = 0$ ), the first particle reaches the wall in about 6 wall units after it is released. The simulation result also shows that before the first particle deposits on the wall, about 400, 650, and 960 particle bounces occur, respectively, for the three coefficients of restitution considered.

Variations of particle trajectory statistics for  $30\text{-}\mu\text{m}$  silicon particles from a point source at a distance of 10 wall units from a gold surface in a horizontal channel including rebound effects are shown in Figure 13. It is observed that, as  $r$  increases, the particle spreading rate increases slightly and the mean path of the particles gets closer to the

wall. The reason for this behavior of the mean particle trajectory is that nearly elastic particles bounce a large number of times before depositing on the wall. As a result, many particles are suspended very near the wall, which causes the mean trajectory to drift toward the wall as  $r$  increases.

### CONCLUSION

In this article the dispersion and deposition of dust particles from a point source in a turbulent channel flow are studied. An empirical mean velocity profile and the experimental data for turbulent intensities are used in these analyses. The instantaneous turbulence fluctuation field is simulated by a con-

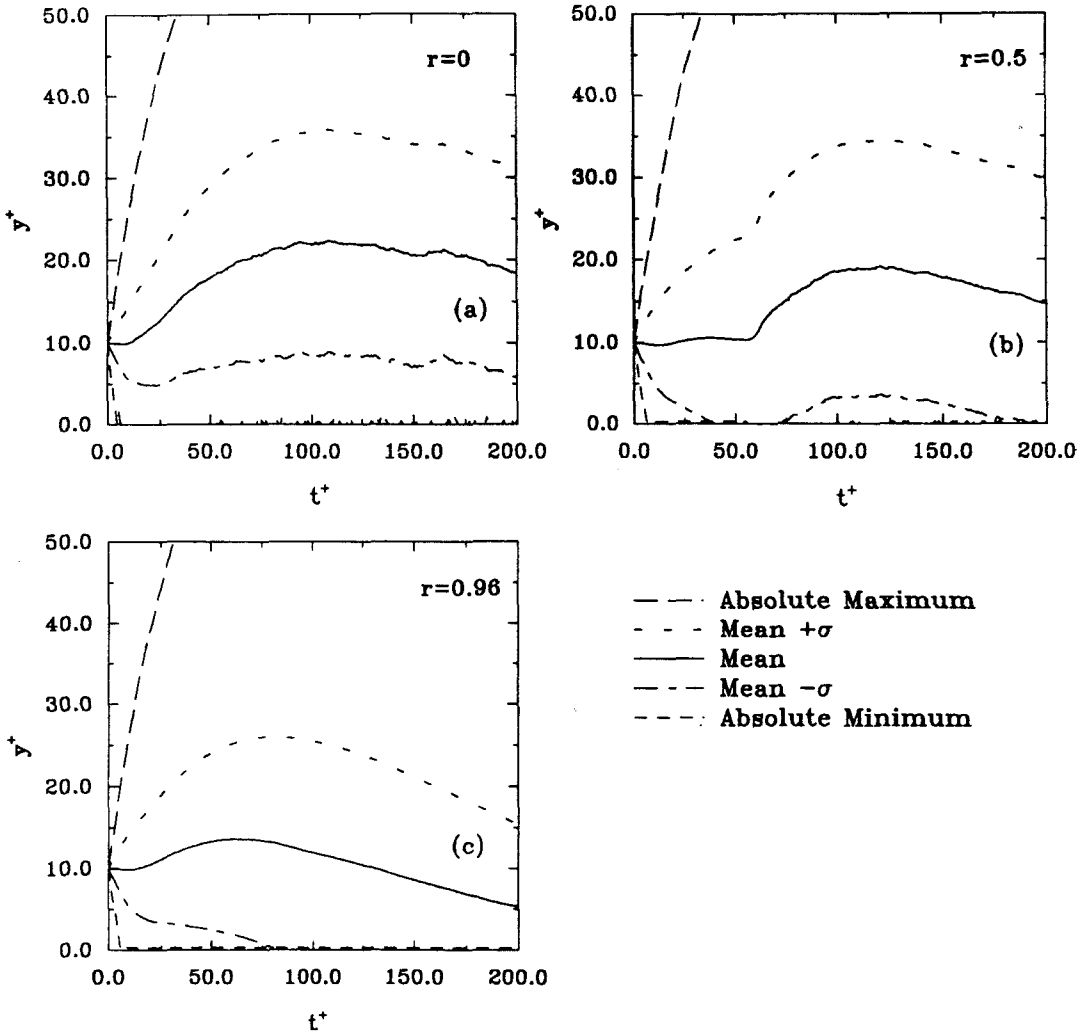


**FIGURE 13.** Particle trajectory statistics including the effect of particle-surface interaction for  $y_0^+ = 1$ .

tinuous Gaussian random field model. The particle equation of motion, which includes the fluid drag and the Brownian and gravitational effects, is solved numerically and ensembles of trajectories for particles of different sizes and densities are generated and statistically analyzed. A series of digital simulations for dispersion and deposition of compact dust particles that are released from point sources at different locations near the wall are performed. Based on the presented

results the following conclusions may be drawn:

1. Variation of deposition rate of particles with size follows a  $V$ -shaped curve with its minimum being about  $0.5 \mu\text{m}$ .
2. For particles larger than  $1 \mu\text{m}$  the deposition rate increases rapidly with particle size.
3. Brownian force significantly affects the dispersion of small particles (with  $d \leq$

- 0.05  $\mu\text{m}$ ) within the inner region of viscous sublayer of about 1 wall unit from the surface.
4. Small particle deposition rate increases rapidly with a decrease in particle diameter.
  5. Particle deposition rate increased sharply with reduction of the source distance from the wall.
  6. Except for the region very near the wall, turbulence is the dominating dispersing mechanism.
  7. Within 1 wall unit from the surface, the turbulence fluctuation effects on submicron particle dispersion are small.
  8. Gravity is the dominating mechanism for deposition of particles larger than 2  $\mu\text{m}$  within 1 wall unit from the surface.
  9. Particle rebound effects cause slight increase in the particle spreading rate and also lead to a drift of mean particle trajectory toward the wall.
  10. An increase of the coefficient of restitution significantly reduces the number of deposited particles.

Thanks is given to Mr. Raymond G. Bayer and Mr. Michael A. Gaynes of IBM—Endicott for their many helpful suggestions and comments. The financial support by IBM—Endicott is also gratefully acknowledged.

## REFERENCES

- Abuzeid, S., Busnaina, A. A., and Ahmadi, G. (1989). *Particulate Science and Technology*, submitted.
- Abuzeid, S., Busnaina, A. A., and Ahmadi, G. (1991). *J. Aerosol Sci.* 22:43–62.
- Ahmadi, G. (1972). *Iranian J. Sci. Tech.* 4:301–310.
- Ahmadi, G. and Goldschmidt, V. (1970). *J. Appl. Mech. ASME* 2:561–563.
- Ahmadi, G., Goldschmidt, V. W., and Dean, B. (1976). *Iranian J. Science and Technology* 5:147–158.
- Browne, L. W. B. (1974). *Atmospheric Environment* 8:801–816.
- Chandrasekhar, S. (1943). *Reviews of Modern Physics* 15:1–89.
- Cleaver, J. W. and Yates, B. (1975). *Chemical Eng. Sci.* 30:983–992.
- Cooper, D. W. (1986). *Aerosol Sci. Technol.* 5:287–299.
- Cooper, D. W., Peters, M. H., and Miller, R. J. (1989). *Aerosol Sci. Technol.* 11:133–143.
- Dahneke, B. (1971). *Colloid and Interface Sci.* 37:342–353.
- Dahneke, B. (1972). *Colloid and Interface Sci.* 40:1–13.
- Davies, C. N. (1966). *Aerosol Science*, Academic Press, London.
- Davies, J. T. (1972). *Turbulence Phenomena*, Academic Press, New York.
- Davis, R. H. et al. (1986). *J. Fluid Mech.* 163:479–497.
- Einstein, A. (1903). *Ann. D. Physik.* 17:549.
- Friedlander, S. K. (1977). *Smokes, Dust, and Haze*, John Wiley, New York.
- Friedlander, S. K. and Johnstone, H. H. (1957). *Ind. Eng. Chem.* 49:1151.
- Fuchs, N. A. (1964). *The Mechanics of Aerosol*, Pergamon, Oxford.
- Goldman, B. I. and Marchello, M. J. (1969). *Int. J. Heat and Mass Transfer* 12:797–802.
- Gupta, D. and Peters, M. (1985). *Colloid and Interface Sci.* 104.
- Hidy, G. M. (1984). *Aerosols, An Industrial and Environmental Science*, Academic Press, New York.
- Hinze, J. O. (1975). *Turbulence*, McGraw-Hill, New York.
- Kraichnan, R. H. (1970). *Phys. Fluid.* 11:22–31.
- Kreplin, H. P. and Eckelmann, H. (1979). *Physics Fluids* 22:1233–1239.
- Laufer, J. (1953). Report 1053, pp. 1247, National Advisory Committee for Aeronautics.
- Levich, V. G. (1962). *Physicochemical Hydrodynamics*, Prentice-Hall, Englewood Cliffs, NJ.
- Liu, B. Y. H. and Kang-ho, Ahn. (1987). *Aerosol Sci. Technol.* 6:215–224.
- Maxey, M. R. and Riley, J. J. (1983). *Phys. Fluid* 26:883–889.
- McLaughlin, J. B. (1989). *Phys. Fluids A* 1:1211–1224.
- Ounis, H. and Ahmadi, G. (1990). *J. Fluids Engineering* 112:114–120.
- Ounis, H., Ahmadi, G., and McLaughlin, J. B. (1991). *J. Colloid and Interface Sci.* 143:266–277.
- Papavergos, P. G. and Hedley, A. B. (1984). *Chem. Eng. Des.* 62:275–295.
- Peskin, R. L. (1975). *International Association for Mathematics and Computers in Simulations*, Rutgers University, New Brunswick, NJ, 207–214.
- Riley, J. J. (1971). Ph.D. Dissertation, Johns Hopkins University, Baltimore, MD.
- Rizk, M. A. and Elghobashi, S. E. (1985). *Phys. Fluid* 20:806–817.
- Saffman, P. G. (1965). *J. Fluid Mech.* 22:385–398.
- Sehmel, G. A. (1973). *Aerosol Science* 4:125–138.
- Uhlenbeck, E. G. and Ornstein, S. L. (1930). *Physics Review* 36:823–841.
- White, F. M. (1986). *Fluid Mechanics*, McGraw-Hill, New York.
- Wood, N. B. (1981a). *J. Aerosol Sci.* 12:275–290.
- Wood, N. B. (1981b). *J. Inst. Energy* 76:76–93.

Received July 17, 1991; accepted November 22, 1991.